BIOMOLECULES & THERAPEUTICS

Original Article
Biomol Ther 27(6), 530-539 (2019)

Etoposide Induces Mitochondrial Dysfunction and Cellular Senescence in Primary Cultured Rat Astrocytes

Minji Bang, Do Gyeong Kim, Edson Luck Gonzales, Kyoung Ja Kwon* and Chan Young Shin*

Department of Neuroscience, School of Medicine and Center for Neuroscience Research, Konkuk University, Seoul 05029, Republic of Korea

Abstract

Brain aging is an inevitable process characterized by structural and functional changes and is a major risk factor for neurodegenerative diseases. Most brain aging studies are focused on neurons and less on astrocytes which are the most abundant cells in the brain known to be in charge of various functions including the maintenance of brain physical formation, ion homeostasis, and secretion of various extracellular matrix proteins. Altered mitochondrial dynamics, defective mitophagy or mitochondrial damages are causative factors of mitochondrial dysfunction, which is linked to age-related disorders. Etoposide is an anti-cancer reagent which can induce DNA stress and cellular senescence of cancer cell lines. In this study, we investigated whether etoposide induces senescence and functional alterations in cultured rat astrocytes. Senescence-associated β-galactosidase (SA-β-gal) activity was used as a cellular senescence marker. The results indicated that etoposide-treated astrocytes showed cellular senescence phenotypes including increased SA-β-gal-positive cells number, increased nuclear size and increased senescence-associated secretory phenotypes (SASP) such as IL-6. We also observed a decreased expression of cell cycle markers, including Phospho-Histone H3/Histone H3 and CDK2, and dysregulation of cellular functions based on wound-healing, neuronal protection, and phagocytosis assays. Finally, mitochondrial dysfunction was noted through the determination of mitochondrial membrane potential using tetramethylrhodamine methyl ester (TMRM) and the measurement of mitochondrial oxygen consumption rate (OCR). These data suggest that etoposide can induce cellular senescence and mitochondrial dysfunction in astrocytes which may have implications in brain aging and neurodegenerative conditions.

Key Words: Astrocytes, Energy homeostasis, Mitochondria, Cellular Senescence, Phagocytosis, Wound Healing

INTRODUCTION

Astrocytes are the most abundant cells in the brain and serve various functions including the maintenance of brain physical formation, ion homeostasis, and secretion of various extracellular matrix proteins (Burda *et al*., 2016). Astrocytes act as helpers to surrounding neurons and aids for cell growth and survival by secretion of extracellular matrix and neurotrophic factors. They are also involved in the signal transduction of neurons through the regulation of ion and neurotransmitter concentrations including glutamate (Fiacco *et al*., 2009). Astrocytes, along with microglia, regulate the brain immune system and maintain the function of the blood-brain barrier (BBB) (Abbott, 2002). Through these roles, any dysfunction of astrocytes can affect various brain cells and the overall brain environment (Dossi *et al*., 2018).

The maintenance of neural environment by the astrocytes requires a continuous and efficient supply of energy, and mitochondria are crucial for this function (Voloboueva *et al*., 2007). Cellular damage and reduction of energy production through increased reactive oxygen species during the aging process are linked to the mitochondria, which may underlie the age-related degenerative changes in the brain. However, mechanistic studies on astrocytic mitochondrial dysfunction related to aging are scarce compared to neurons.

In the brains of Alzheimer's disease patients as well as in aged subjects, increased expression of senescent astrocytes as well as changes in astrocyte morphology has been reported (Bhat *et al*., 2012). Aged astrocytes are known to increase the number of SA-β-gal-positive cells with a flattened

Open Access **https://doi.org/10.4062/biomolther.2019.151**

Received Sep 16, 2019 **Revised** Sep 23, 2019 **Accepted** Sep 25, 2019
Published Online Oct 24, 2019

***Corresponding Authors**
E-mail: chanyshin@kku.ac.kr (Shin CY), kjjasmine@hanmail.net (Kwon KJ)
Tel: +82-2-2030-7834 (Shin CY), +82-2-454-5630 (Kwon KJ)
Fax: +82-2-2049-6192 (Shin CY), +82-2-2030-7899 (Kwon KJ)

morphology according to a previous report (Bhat *et al*., 2012). However, cellular senescence phenotypes vary depending on cell types and the methods inducing cellular senescence. Cellular senescence is the most well-characterized and studied area in cancer cell biology. Cancer cells show changes in senescence-associated secretory phenotypes (SASP) under cellular senescence conditions. Similarly, aged astrocytes can also alter the expression of dozens of SASP factors including TNF-α, IL-1β, IL-6 and HMGB1 (Enokido *et al*., 2008; Campuzano *et al*., 2009; Campisi *et al*., 2011; Salminen *et al*., 2011; Bhat *et al*., 2012; Hou *et al*., 2018). Despite the obvious importance of the aging process of astrocytes in the brain, relatively few studies have been conducted on astrocyte senescence compared to neuronal senescence.

To induce cellular senescence, various methods have been adopted by researchers. One of the commonly used methods is the use of chemicals, such as etoposide and doxorubicin, which can induce cellular senescence. Etoposide is an anticancer drug against various types of cancer and is known to induce senescence by DNA damage (te Poele *et al*., 2002; Nasrin Ghassemi and Shokrzadeh, 2018). Etoposide is a DNA topoisomerase inhibitor that breaks the DNA double-stranded structure and blocks repair by topoisomerase II-binding (Pommier *et al*., 2010). In this study, we induced cellular senescence in astrocytes by etoposide treatment and investigated any specific changes in astrocytic function or morphology. We also identified the alteration of mitochondrial function in senescent astrocytes. The dysfunction of energy homeostasis in astrocytes may act as a key determinant of the aged phenotypes of the brain.

MATERIALS AND METHODS

Materials

The materials and their manufacturers' information used in this study are the following: Dulbecco's modified Eagle medium (DMEM)/F12, Penicillin-Streptomycin (P/S), 0.25% trypsin-EDTA and 10% Fetal Bovine Serum (FBS) from Gibco BRL (Grand Island, NY, USA); dimethyl sulfoxide from Invitrogen (Carlsbad, CA, USA); Tween® 20 and ECLTM Western blotting detection reagent from Amersham Life Science (Arlington Heights, IL, USA); etoposide from Selleckchem.com (Houston, TX, USA); anti-β Actin from Sigma (St. Louis, MO, USA); anti-Phospho-Histone H3 and anti-Histone H3 from Cell Signaling Technology (MA, USA); anti-CDK2 and anti-CDK4 from Santa Cruz Biotechnology; anti-GFAP from EMD Millipore (MA, USA); senescence detection kit from Abcam; Agilent Seahorse XF Cell Mito Test Kit from Agilent Technology (CA, USA); Doxorubicin from Sigma; Alexa Fluor® 594 conjugated Escherichia coli (K-12 strain) BioParticles® from Thermo Fisher Scientific (MA, USA); Tetramethylrhodamine Methyl Ester (TMRM) from Thermo Fisher Scientific.

Astrocytes culture

Animal experiment procedures were carried out following the protocols approved by the Institutional Animal Care and Use Committee (IACUC) of Konkuk University (KU18050). Sprague-Dawley (SD) rats were bought from Samtako, Inc (Gyeonggi, Korea). Astrocytes were cultured from the brain cortex of postnatal day 2 (P2) SD rats as described previously (Kim *et al*., 2013). Briefly, brain cortices were isolated and mechanically triturated into single cells. Cells were seeded on the poly-D-lysine-coated plate (20 μg/ml) and maintained in DMEM/F12 with 100 U/ml of penicillin, 100 mg/ml of streptomycin, and 10% heat-inactivated FBS in a 95% CO_2 incubator at 37°C. The medium of the cultured astrocyte was changed every 4 days. After 2 weeks, the confluent cells were washed twice with serum-free medium and detached by 0.25% trypsin-EDTA. The isolated astrocytes were sub-cultured by re-plating in 6, 12, 24, or 96-well plates. The sub-cultured astrocytes were positive for GFAP and the astrocyte purity was more than 95%.

Neuron culture

Sprague-Dawley (SD) rats were purchased from ORIENT (Gyeonggi, Korea). The primary cortical neurons were isolated from the cerebral cortex of embryonic day 17 (E17) SD rats. The isolated cortical neurons were seeded on the poly-D-lysine-coated plate (50 μg/ml) and incubated in NBM with B27 and L-glutamine in a 95% CO_2 incubator at 37°C for 10 days and the media were half-replaced with fresh ones every 3 days.

Etoposide treatment

The cultured astrocytes were treated with either 1 or 10 μM etoposide for 24 h. The vehicle group was treated with 0.1% DMSO. In wound scratch assay, 10 μM of etoposide was treated and examined for 72 h. In these experiments, no cellular toxicity was observed by PI (propidium iodide) staining (data not shown).

Senescence-associated-β-galactosidase (SA-β-gal) staining

SA-β-gal staining was performed using Senescence Detection Kit (Abcam, Cambridge, UK) to detect SA-β-gal activity in cultured cells. The experimental procedures were performed following the manufacturer's instructions (Dimri *et al*., 1995). Astrocytes were seeded in 12-well plates at 2.5×10^5 cells/well. After 4 days, the confluent cells were used in the experiments. The SA-β-gal-positive cells were observed with bright-field microscopy.

Nuclear staining

The cultured cells were grown on a poly-D-lysine-coated coverslip and fixed by 4% paraformaldehyde (PFA) for 10 min at 37°C. After then, the cells were permeabilized with 0.1% Triton X-100 for 20 min at room temperature and washed 3 times with PBS. The fixed cells were stained for 10 min at room temperature with DAPI. After then, the cells were mounted and visualized by a digital microscope (CELENA, Logos Biosystems, Gyeonggi, Korea). The nuclear size was measured using the Image J software (NIH, MD, USA).

Reverse transcription-polymerase chain reaction (RT-PCR)

The expression of selected mRNAs in astrocytes such as IL-1β, IL-6, TNFα, iNOS, p21, p16, p53, and GAPDH were detected using RT-PCR. The RNA was extracted with TRIzol reagent (Invitrogen) and the concentration was measured using a spectrophotometer (Nanodrop Technologies, Wilmington, DE, USA). cDNA synthesis was performed using RNA and RT reaction mixture with RevertAid Reverse transcriptase reaction buffer (Thermo Fisher Scientific) and dNTP (Promega, WI, USA). A total of 0.5 μl of cDNA samples were utilized

for PCR amplification under the following cycle parameters: [94°C, 30 s; 60°C, 1 min; 72°C, 30 s]×30 cycles, then 72°C for 10 min to detect IL-1β, IL-6, TNFα, iNOS, p21, p16 and p53; and [94°C, 30 s; 60°C, 1 min; 72°C, 30 s]×23 cycles, then 72°C for 10 min to detect GAPDH. The primers were designed for the following: IL-1β (sense: 5'-AAA ATG CCT CGT GCT GTC TG-3'/ antisense: 5'-CTA TGT CCC GAC CAT TGC TG-3'), IL-6 (sense: 5'-TTG TGC AAT GGC AAT TCT GA-3'/ antisense: 5'-TGG AAG TTG GGG TAG GAA GG-3'), TNFα (sense: 5'-TAG CCC ACG TCG TAG CAA AC-3'/ antisense: 5'-GGA GGC TGA CTT TCT CCT GG-3'), iNOS (sense: 5'- CTG GCT GCC TTG TTC AGC TA-3'/ antisense: 5'-AGT GTA GCG TTT CGG GAT CT-3'), p21 (sense: 5'-GGA CAG TGA GCA GTT GAG CC-3'/ antisense: 5'-ACA CGC TCC CAG ACG TAG TT-3'), p16 (sense: 5'-ATC TCC GAG AGG AAG GCG AAC TCG-3'/ antisense: 5'-TCT GTC CCT CCC TCC CTC TGC TAA C-3'), p53 (sense: 5'-TAT GAG CCA CCT GAG GTC GG-3'/ antisense: 5'-TCT CCC AGG ACA GGC ACA AA-3'), and GAPDH (sense: 5'-GTG AAG GTC GGT GTG AAC GGA TTT-3'/ antisense: 5'-CAC AGT CTT CTG AGT GGC AGT GAT-3'). The PCR products were electrophoresed with 1.2% agarose gel and visualized with ethidium bromide (Sigma). The bands were measured using the Image J software (NIH). Each band intensity was normalized using GAPDH mRNA.

Western blot analysis

Western blot analysis was performed following a published protocol described previously (Bang *et al*., 2018). Briefly, the cells were harvested with radioimmunoprecipitation assay (RIPA) buffer consisting of 2 mM EDTA, 0.1% (w/v) SDS, 50 mM Tris-HCl, 150 mM sodium chloride, 1% Triton X-100, and 1% (w/v) sodium deoxycholate. The extracted proteins were quantified by BCA assay kit (Thermo Fisher Scientific) and boiled for 5 min at 100°C. The SDS-PAGE was conducted for 120 min at 100 V. The electrophoresed samples were transferred to nitrocellulose membranes for 90 min and the proteins were blocked with 1 μg/ml polyvinyl alcohol for 5 min at room temperature and then washed with Tris-buffered saline and 0.1% Tween 20 (TBS-T). Afterward, the samples were incubated with their designated primary antibodies for 16 h at 4°C. The samples were again washed and incubated with horseradish peroxidase-conjugated secondary antibody (Life Technologies, Carlsbad, CA, USA) at room temperature for 60 min. The protein blots were detected by a chemiluminescence detection system (Amersham, Buckinghamshire, UK) and quantified using Image-J software (NIH). β-Actin was used as the loading control.

Wound closure assay

To analyze wound closure, astrocytes were seeded on poly-D-lysine-coated 96-well plates at a density of 2.5×10^5 cells/ml and incubated for 4 days until they reached confluence. After then, a 700 nm-wide scratch was made in each well using a certified Essen Biosciences automated 96-wound-maker™ (Essen Biosciences, Hertfordshire, UK). Wound closure was measured using the IncuCyte ZOOM system (Essen Bioscience) by imaging each well every 3 h for 72 h. The wound width and relative wound density data were analyzed using the IncuCyte ZOOM microscope software 2015A (Essen Bioscience). The relative wound density was defined as the cell density in the wound area relative to the cell density outside of the wound area over time. This metric was normalized for changes in cell density by proliferation and/or pharmacological effects.

Phagocytosis

Alexa Fluor™ 594 conjugated *Escherichia coli* (K-12 strain) BioParticles™ were used for confirming phagocytosis activity in astrocytes. The astrocytes were incubated with *E. coli* BioParticles for 12 h in a 95% CO_2 incubator at 37°C. We measured the red fluorescence using the IncuCyte ZOOM system (Essen Bioscience) by imaging each well every 10 min for 12 h, and then analyzed by the IncuCyte ZOOM microscope software 2015A (Essen Bioscience).

Determination of mitochondrial membrane potential

The mitochondrial function was identified by membrane potential fluorescence staining using TMRM. TMRM is a dye that penetrates into the cells and accumulates in the mitochondria which have active membrane potentials. If cells are healthy and functioning, signals will shine brightly, while if the membrane potential is decreased, signals will reduce or disappear. Astrocytes were incubated with 100 nM TMRM for 30 min in a 95% CO_2 incubator and light protection condition at 37°C. After then, the samples were washed with phosphate-buffered saline (PBS) and visualized by digital microscope (CELENA, Logos Biosystems).

Mitochondrial oxygen consumption rate (OCR)

The mitochondrial OCR of cells was determined following

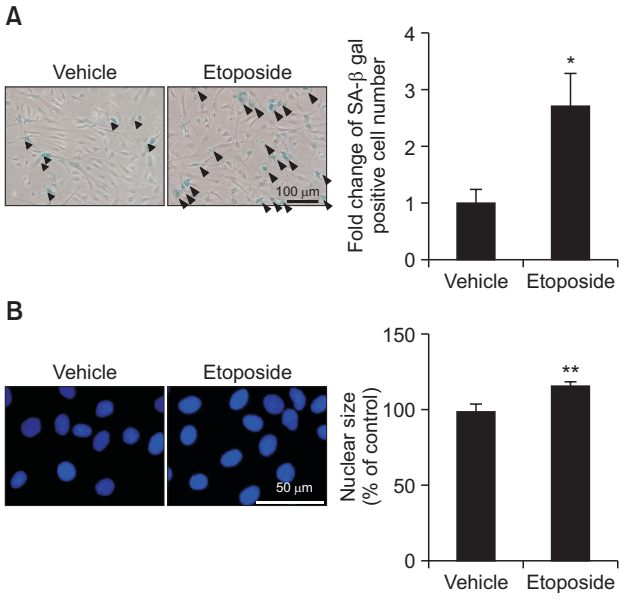

Fig. 1. Morphological changes of etoposide-treated astrocytes *in vitro*. (A) Astrocytes were stained to determine the activity of senescence-associated beta-galactosidase (SA-β-gal). Astrocytes were treated with DMSO (vehicle) or 10 μM etoposide for 24 h. Stained astrocytes were taken at 100x magnification and black triangles indicate SA-β-gal-positive cells. The graph represents the fold change in SA-β-gal-positive cell number in 10 μM etoposide-treated astrocytes. (B) Astrocytes were stained to determine the nuclear size. The graph presents the percent of nuclear size compared to control. The bars represent the mean ± SEM. * indicates $p<0.05$ and, ** indicates $p<0.01$ vs. vehicle group.

the Agilent Seahorse XF Cell Mito Test Kit user guide (Agilent Technology). Briefly, we hydrated the cartridge with a calibrant buffer in a non-CO_2 incubator at 37°C, overnight before the assay. A mixture of 1.0 μM oligomycin, 1.0 μM FCCP, and 0.5 μM rotenone/0.5 μM antimycin A was added into the cartridge port A to C, respectively. The cell culture growth medium was changed into 1 mM pyruvate, 2 mM glutamine, and 10 mM glucose-containing Seahorse XF Base Medium and was incubated for 45 min to 1 h prior to the assay. The experiments were conducted using Agilent Seahorse XFe96 Analyzer (Agilent Technology). The results were exported using Wave Desktop 2.6 software (Agilent Technology) and calculated using the Agilent Seahorse XF Cell Mito Test Kit user guide (Agilent Technology).

MTT assay

To confirm the neuronal cell-protection ability of astrocytes under cell death condition, we performed an MTT assay in primary cultured neurons within the astrocyte conditioned medium (ACM). Neurons were treated with ACM for 48 h at day-in-vitro 7 (DIV7). And then, a 0.1 mg/ml MTT solution was treated in the medium of primary cultured neurons for 1 h in a 95% CO_2 incubator and light-protection condition at 37°C. The incubated medium was changed to DMSO before the absorbance was measured at OD=570 nm.

Statistical analysis

All the experimental results were expressed as the mean ± SEM and the statistical analyses were performed using GraphPad Prism 5 software (GraphPad Software Inc., CA, USA). The data comparisons were performed using two-way ANOVA followed by Bonferroni's post-test in comparing grouped samples. Three-sample analyses were performed with one-way ANOVA, and two-sample analyses were done with unpaired *t*-test. A *p*-value of <0.05 was considered significant.

RESULTS

Etoposide induces SA-β-gal activity and increases the nuclear size in cultured rat astrocytes

We performed SA-β-gal staining to determine whether etoposide-treated astrocytes induce cellular senescence. The increased activity of SA-β-gal, a typical aging marker, shows blue granules in the cytosol. When astrocytes were treated with 10 μM of etoposide for 24 h, the number of SA-β-gal positive cells was significantly increased to about 3 folds compared to the vehicle group (black triangles, Fig. 1A). Based on the reports of nuclear enlargement in senescent cells (Yoon *et al*., 2016), we determined any change of nuclear size by DAPI staining assay in etoposide-treated astrocytes. Treatment with

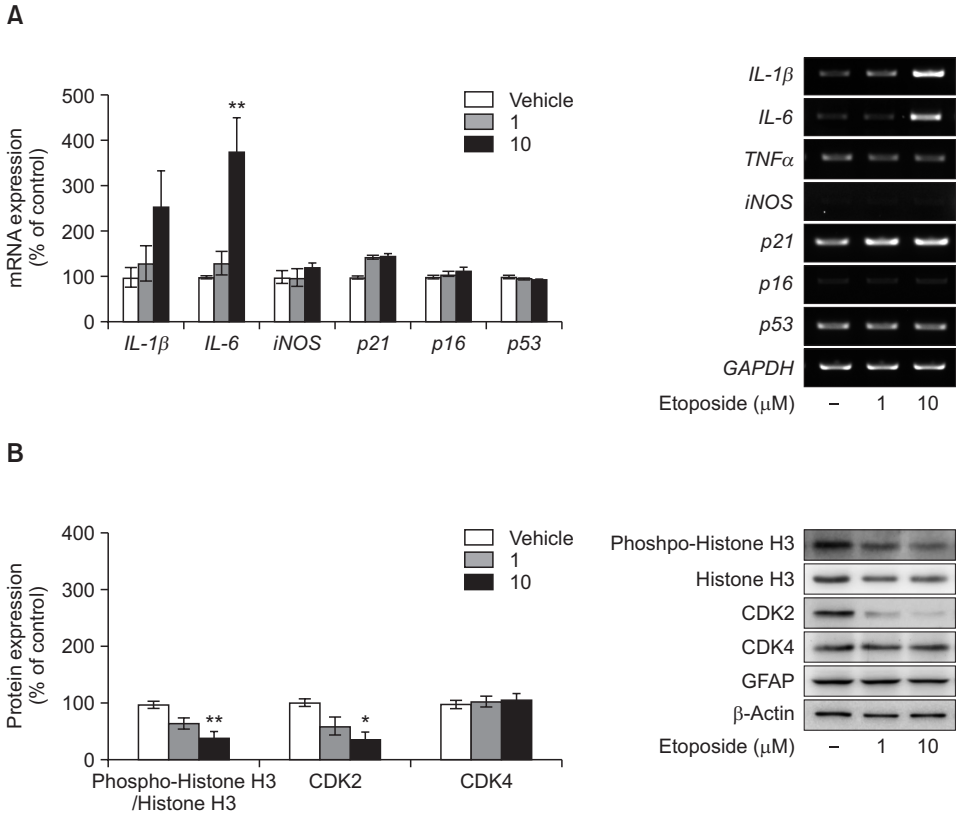

Fig. 2. Expression of inflammatory and cell cycle markers in etoposide-treated astrocytes *in vitro*. Rat primary cultured astrocytes were treated with DMSO (vehicle), etoposide 1 μM, or etoposide 10 μM for 24 h. (A) The expression level of senescence-related genes was measured by reverse transcription PCR (RT-PCR). The graph represents the mRNA expression levels. Values were normalized based on GAPDH. (B) The expression level of senescence-related proteins was measured by Western blot. Densitometry analysis of the protein expression levels. The graph represents the protein expression levels and the values were normalized to the Actin expression. The bars represent the mean ± SEM. * indicates $p<0.05$ and ** indicates $p<0.01$ vs. vehicle group.

10 μM etoposide in astrocytes for 24 h increased the size of stained DAPI for about 15 percent compared to the vehicle group (Fig. 1B). These results suggest that the etoposide-treated senescent astrocytes show morphological features similar to that of senescent cells.

Etoposide modulates the gene expression of immune and cell cycle-related factors in astrocytes

To confirm whether the etoposide-treated astrocytes exhibit molecular features of senescent cells, we examined their expression of senescent cell-related factors. In the 10 μM etoposide-treated astrocytes, IL-6 mRNA expression was increased for about 4 folds (Fig. 2A). In addition, the Western blot analysis revealed that the protein level of Phospho-Histone H3/Histone H3 and CDK2, which are related to the regulation of cell cycle progression, were dose-dependently decreased. Moreover, the highest concentration of etoposide treatment reduced the protein expression of Phospho-Histone H3/Histone H3 and CDK2 for about 60 percent (Fig. 2B).

Etoposide dysregulates wound-healing ability and phagocytosis in astrocytes

We further examined other functional changes of senescent astrocytes. First, we performed wound-scratch assay to measure any changes in their wound-healing ability. In the early stage, all the treatment conditions of astrocytes have similar wound closure ability. Interestingly, differences were observed after 30 to 33 h when the etoposide-treated astrocytes displayed a reduction in wound-healing ability (Fig. 3A), wider wound width (Fig. 3B), and lower wound density (Fig. 3C). Relative wound density was defined as the cell density in the wound area relative to the cell density outside of the wound area over time. This metric was normalized for changes in cell density by proliferation and/or pharmacological effects.

Furthermore, changes in phagocytosis capacity in etoposide-treated astrocytes were confirmed using *E. coli* BioParticles (Fig. 3D). Etoposide-treated astrocytes showed a decreased red fluorescence between 8 h and 20 min to 50 min (Fig. 3E). The total fluorescence intensity was significantly decreased in the etoposide-treated astrocytes between 5 h and 30 min to 8 h and 20 min (Fig. 3F), but not afterward.

Etoposide-treated astrocytes exhibited mitochondrial dysregulation phenotypes

To check any changes in the mitochondrial function of senescent astrocytes by etoposide treatment, we measured the

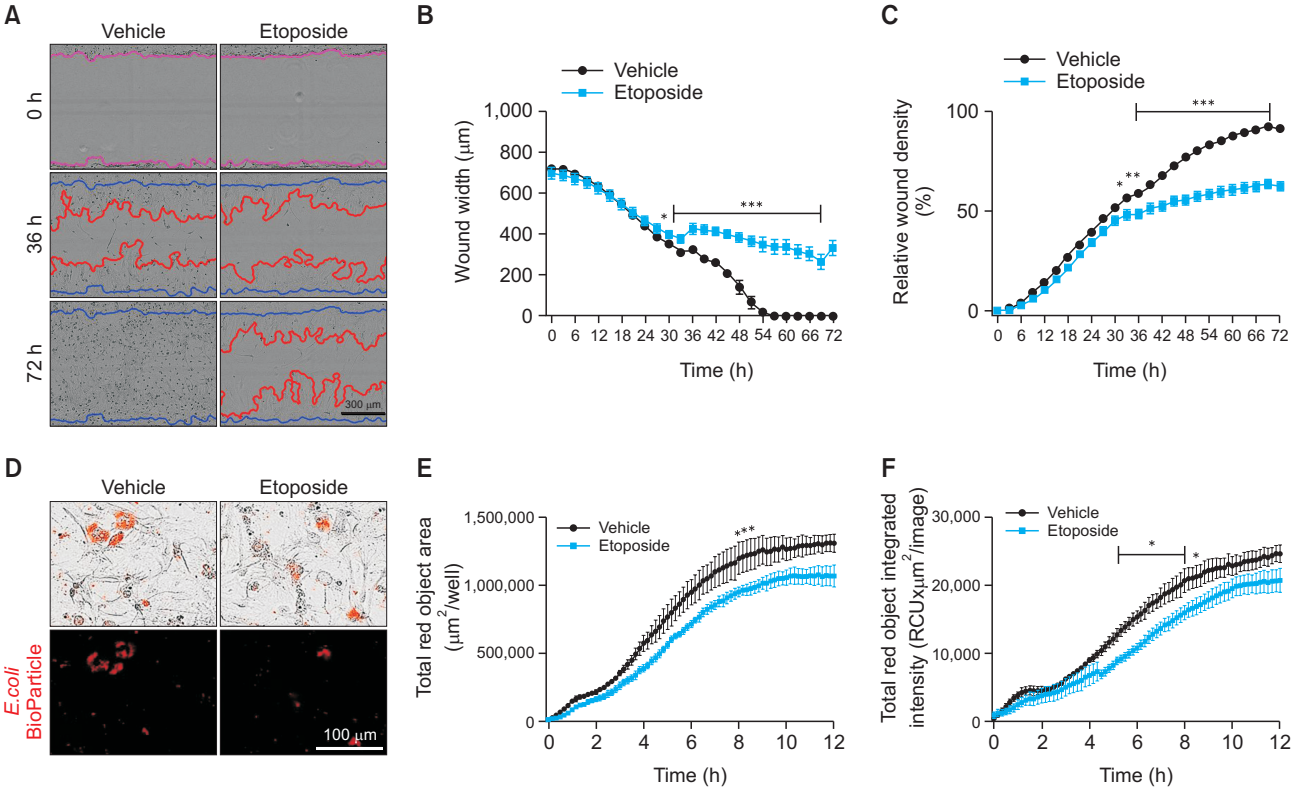

Fig. 3. Cellular functional changes of etoposide-treated astrocytes *in vitro*. Scratch wound assay (A-D). The monolayer of rat primary cultured astrocytes were treated with DMSO (vehicle) or 10 μM etoposide for 72 h. (A) Representative images of astrocytes in the wound-healing assay. Blue lines indicate the initial scratch-wound area. Red lines show wound closure at each time-point. Images and data obtained using IncuCyte (Essen Bioscience) under the 10x object. (B) Cell migration every 3 h into the wound area, represented by wound width (μm) in the modified scratch-wound assay analysis. (C) The percentage of relative wound density in the scratch wound area was determined. (D) Etoposide-treated cells were assessed for its phagocytosis ability using *E. coli* BioParticles. Astrocytes were treated with DMSO (vehicle) or 10 μM etoposide for 12 h. (E) The graph shows total red object area per well (μm^2/well) every 10 min for 12 h. (F) The representative graph shows the total red object integrated intensity (RCU x μm^2/image) every 10 min for 12 h. Lines represent the mean ± SEM. * indicates $p<0.05$, ** indicates $p<0.01$, and *** indicates $p<0.001$ vs. vehicle group.

membrane potential of astrocytes using a fluorescence indicator. Etoposide-treated astrocytes were observed using the TMRM dye staining (Fig. 4A). In this study, astrocytes were treated with etoposide for 24 h. The TMRM dye shows a red stain object and the etoposide-treated astrocytes show significantly decreased total red object integrated intensity (Fig. 4B), and total red object area than the vehicle group after 24 h treatment (Fig. 4C). Doxorubicin was used as a positive control. Similarly, we detected the mitochondrial oxygen consumption rate using Agilent Seahorse XFe96 Analyzer (Agilent Technology) to determine whether etoposide-induced astrocyte senescence affects mitochondrial function (Fig. 4D). Oligomycin, FCCP, and rotenone/antimycin A were sequentially treated to astrocytes to determine their ATP production, maximal respiration, and non-mitochondrial respiration, respectively. Consequently, the etoposide-treated astrocytes exhibited down-regulated basal respiration and decreased ATP production (Fig. 4E, 4F). These values of basal respiration and decreased ATP production are used for calculating proton leak and spare respiratory capacity. We also confirmed that the spare respiratory capacity was decreased in the etoposide-induced senescent astrocytes (Fig. 4E, 4F).

Conditioned media of etoposide-treated astrocytes adversely affect neuronal function

Astrocytes were treated with etoposide for 48 h followed by incubation for another 48 h, after washing, to obtain senescent astrocyte conditioned media (ACM) without etoposide. ACM was applied to neurons to confirm changes in cellular supportive functions of senescent astrocytes. After ACM treatment, the neurons were given 100 μM H_2O_2 to stimulate oxidative stress. There was no difference in the cell viability of neurons in the fresh media-treated group (No ACM), vehicle-treated ACM group (Veh-ACM) and etoposide-treated ACM group (Eto-ACM) without H_2O_2 treatment. However, when treated with 100 μM H_2O_2, the cell viability of No ACM and Eto-ACM group was decreased to about 55% while the Veh-ACM condition slightly prevented this observed decrease. In addition, the Eto-ACM condition has slightly further reduced the cell viability of neurons in the H_2O_2 challenge, suggesting absence of any protective effect may result in the loss of neuroprotective function in astrocytes treated with etoposide (Fig. 5A).

To determine the mitochondrial functional changes of neurons by ACM treatment, we measured the mitochondrial OCR in neurons treated with No ACM, Veh-ACM, or Eto-ACM (Fig. 5B). Eto-ACM treated neurons showed decreased basal respiration and ATP production than Veh-ACM (Fig. 5C, 5D). The measured values were further calculated for proton leak and

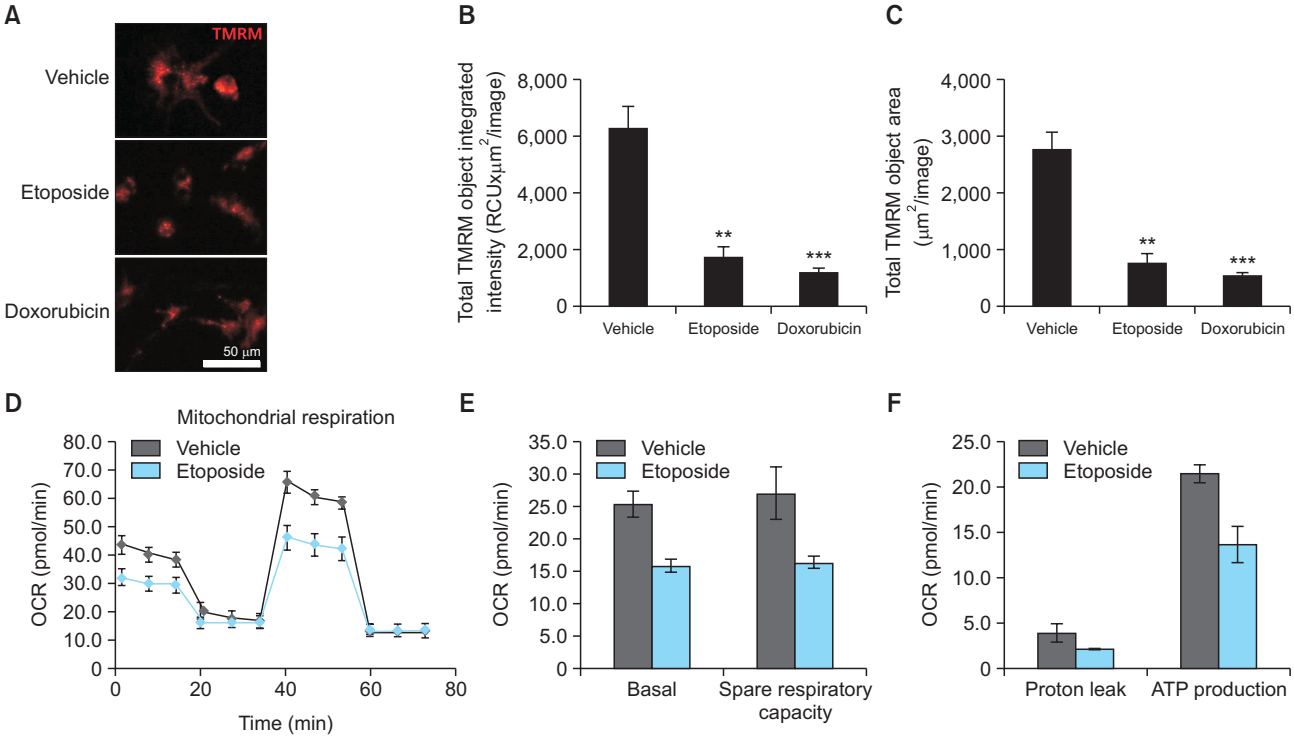

Fig. 4. Functional changes of mitochondria in etoposide-treated astrocytes. Astrocytes were treated with DMSO (vehicle) or 10 μM etoposide for 24 h. (A) Cultured astrocytes were detected for mitochondrial membrane potential by fluorescence staining of TMRM. Representative images were visualized by the IncuCyte ZOOM microscope software 2015A (Essen Bioscience) under the 20x object. The data were calculated by IncuCyte software (Essen Bioscience). (B) The representative graph indicates the total TMRM object integrated intensity (RCU x μm^2/image). (C) The graph shows the total TMRM object area (μm^2/image) in astrocytes. Bars represent the mean ± SEM. ** indicates $p<0.01$, and *** indicates $p<0.001$ vs. vehicle group. (D) The mitochondrial oxygen consumption rate (OCR) of astrocytes was measured using Cell Mito Test Kit (Agilent Technology) and Agilent Seahorse XFe96 Analyzer (Agilent Technology). The representative graph was obtained using Wave Desktop 2.6 software (Agilent Technology). (E) and (F) graphs show the basal level, spare respiratory capacity, proton leak, and ATP production level.

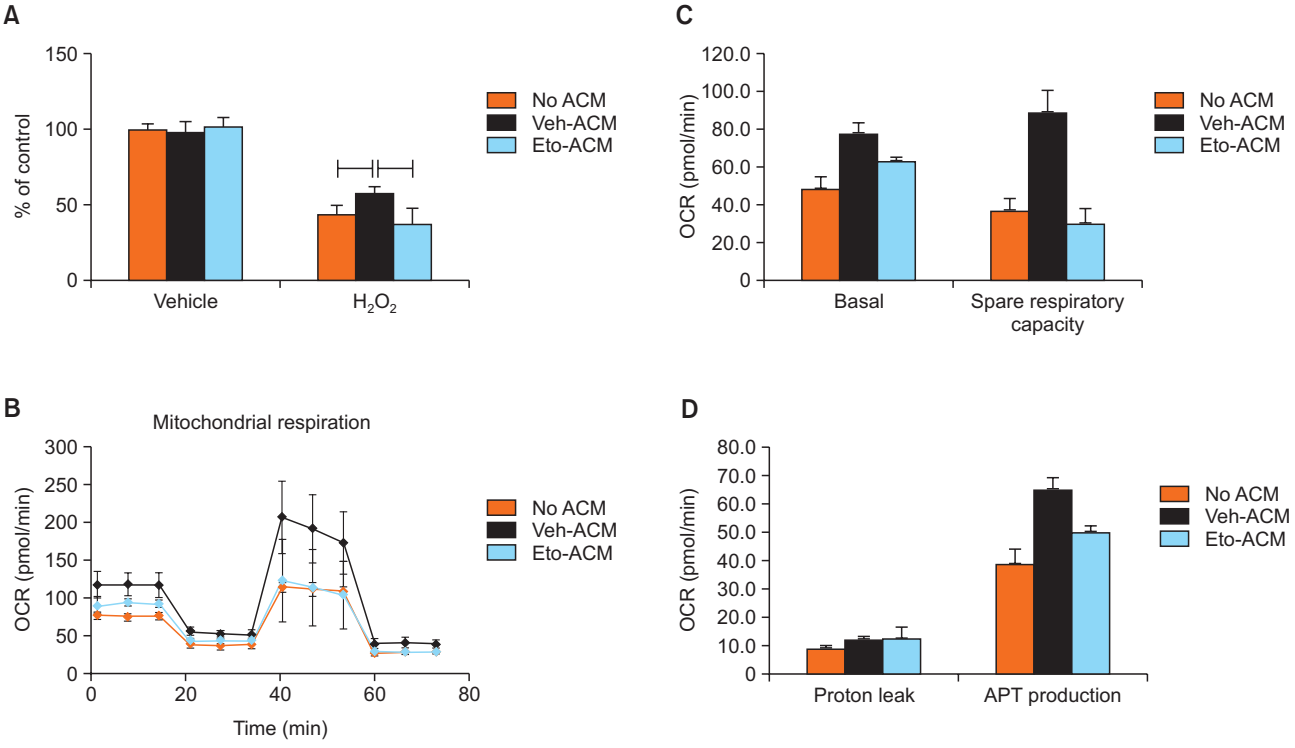

Fig. 5. Effects on neuronal mitochondrial respiration and cell viability by culture-conditioned medium from senescent astrocytes. (A) The cell viability of ACM-treated neurons after H_2O_2 stimulation was determined by MTT assay. Values are expressed as the mean ± SEM. * indicates $p<0.05$, and *** indicates $p<0.001$ vs. no ACM group. (B) Mitochondrial oxygen consumption rate (OCR) was measured in astrocytes by Cell Mito Test Kit (Agilent Technology) and Agilent Seahorse XFe96 Analyzer (Agilent Technology). The representative graph was obtained using Wave Desktop 2.6 software (Agilent Technology). (C, D) The basal level, spare respiratory capacity, proton leak, and ATP production level in neurons treated with ACM from senescent astrocytes.

spare respiratory capacity to which the proton leak was not changed while the spare respiratory capacity was decreased in Eto-ACM treated neurons (Fig. 5C, 5D).

DISCUSSION

Majority of studies about cellular senescence were focused on the cancer cells, and the neuroscience field of aging is mainly concentrated on neurons with a little progress. In this study, we focused our investigation on the effects of senescent astrocytes in the modulation of functional integrity and viability of neurons. We induced astrocyte-senescence using etoposide and confirmed the cellular changes through positive SA-β-gal stains, increased nuclear size and SASP expression such as IL-6, as well as cell cycle dysregulation.

Not all senescent cells show nuclear enlargement, except in specific cell types such as CNS cells and human diploid fibroblasts. In our etoposide-treated astrocytes, the increase in nuclear size could be related to the inhibition of cell division. Etoposide is an intercalating agent that inhibits topoisomerase II by altering the interface between topoisomerase II and DNA. Accordingly, DNA repair is blocked and the cell cycle is arrested in the G2 phase (Hu *et al*., 2018). When DNA replication occurs during the cell cycle, the size of the cell or nucleus is slightly increased (Amodeo and Skotheim, 2016). Thus, it is possible that preventing the cell cycle from entering the M phase could have caused the enlargement of the nucleus in our study. Some researchers have also suggested the possibility that the increase of macromolecule contents (DNA, RNA, and proteins) as a result of aging, may have affected the cell and nuclear growth (De Cecco *et al*., 2011).

The expression level or pattern of cellular senescence biomarkers are different according to the applied methods that induce senescence as well as the cell or tissue types adopted, but usually the reports showed increased expressions of interleukins such as IL-1β, IL-6, or IL-8. Also, the increased expression of tumor suppressors such as p53, p21, and p16 have been noted (Capell *et al*., 2016; Meyer *et al*., 2017; Ortiz-Montero *et al*., 2017). In particular, the increased expression of IL-6 was observed in aged astrocytes, microglia, and neurons. This phenomenon was also observed in the brain of rodents, monkeys, and Alzheimer's disease patients (Hayflick and Moorhead, 1961; Qiu *et al*., 1998). There are several transcription factors that regulate IL-6, of which the NF-kB binding was observed in the aged brain in the IL-6 promoter region (Godbout and Johnson, 2004). In this study, we observed the increased expression of IL-6. In contrast, the expression of tumor suppressors and iNOS were not affected by etoposide. The increased mRNA expression of immune-related factors may have a connection to reactive astrogliosis and astrocyte immune-activation. The aging of astrocytes could increase the production of cytokines (Boisvert *et al*., 2018; Clarke *et al*., 2018). In addition, increases in IL-6 are found in brain trauma,

CNS infections, and Alzheimer's disease (Woodroofe *et al*., 1991; Kalman *et al*., 1997). Transgenic mice whose astrocytes overexpress IL-6 exhibit decreased neurogenesis and developed neurological diseases (Campbell *et al*., 1993; Vallieres *et al*., 2002). Recent studies have reported that IL-6 may inhibit neurogenesis in the aged brain and induces gliogenesis, especially in Alzheimer's disease. In addition, the N-methyl D-aspartate (NMDA) receptor-mediated neurotoxicity was enhanced when chronically exposed to IL-6 (Qiu *et al*., 1998). Therefore, an increased IL-6 in the aged brain may be related to the susceptibility of developing neurological diseases or neuronal dysfunctions.

The concept of cellular senescence was first described by Hayflick and Moorhead (1961). A representative feature of cellular senescence is cell cycle arrest, which is also observed in aged tissues. But, astrogliosis can re-enter cell cycle and proliferation during scar formation. p16 is an identifying factor of cell cycle arrest, and p53 and p21 have also been studied. Cellular senescence is known to increase the expression of p16 in aged tissues (Bhat *et al*., 2012; Hudgins *et al*., 2018). Recently, many studies have been actively conducted to overcome cellular senescence and inhibit aging. Although we did not observe changes in p16, p21, and p53, we observed changes in the protein expression levels of some cell cycle-related factors. At the protein level, the cell cycle-related factors, such as phospho-Histone H3 and CDK2, were dose-dependently decreased in etoposide-treated astrocytes (Fig. 2B). It is well known that CDK2 reduction is one of the typical features of cellular senescence. CDK2 interacts with cyclin E on G1 phase, which is required in transition from G1 phase to S phase, while binding with Cyclin A proceeds through the S phase. The reduced protein expression of CDK2 could affect cell cycle arrest, although the relationship between CDK2 and brain aging is still unclear.

In addition to the morphological and molecular features of senescent cells, etoposide-treated astrocytes also showed a functional change manifested by their reduced wound-healing ability. The results are consistent with our previous reports showing a reduction of wound healing ability in senescence-induced astrocytes by tenovin-1 via changes in the expressions of sirt1 and 2 (Bang *et al*., 2018). It has been reported that aged bone marrow-derived dendritic cells reveal impaired *in vitro* migration (Grolleau-Julius *et al*., 2008) and old tenocytes and satellite cells also show migration defects (Chang *et al*., 2012; Collins-Hooper *et al*., 2012). Although the regulatory mechanism of astrocyte migration has been related to molecular factors such as matrix metalloproteinase (MMP), C3, and CXC chemokines during brain injury or immune-activated condition, the exact mechanism regulating the astrocyte migration is not yet clear. For example, the wound-healing ability of several cell lines, such as 92.1 and Mel 270, were decreased through the down-regulation of MMP 9 and MMP2 (Dai *et al*., 2016). However, some studies have reported an increase in MMP and immune-related factors during cellular senescence (McHugh and Gil, 2018). Further research is needed on the mechanism involved in the senescent astrocyte migration and its functional role.

In this study, we observed a decreased phagocytosis in senescent astrocytes through *E. coli* BioParticles engulfment assay. In Alzheimer's disease, Aβ is known to be accumulated outside the cells and eliminated by astrocyte phagocytosis (Chung *et al*., 2015). However, as the disease progresses, Aβ is not removed smoothly, and the accumulation is known to cause nerve damage. Astrocytes are also known to play a role in the elimination of synapses by TGFβ through the induction of Megf10 and MERTK during the developmental stage (Bialas and Stevens, 2013). MEGF10 and MERTK phagocytic receptors recognize the phosphatidylserine of the target debris, leading to an engulfment process (Chung *et al*., 2013). However, some previous studies observed that the expressions of MEGF10, MERTK, and TGFβ 1-3 were not altered in astrocytes isolated from aged rats, calling for careful study of the relevant mechanisms (Boisvert *et al*., 2018). These results suggest that the regulatory mechanism of astrocytic phagocytosis should be further investigated in the context of aging and neurodegenerative diseases.

Cell damage and decreased energy production by increased reactive oxygen species observed during the aging process are expected to be closely related to the mitochondria. We checked the mitochondrial function of senescent astrocytes using TMRM. The decrease in intensity of TMRM in senescent cells suggests a mitochondrial dysfunction (Fig. 4B, 4C). Then, the mitochondrial OCR was measured to identify more detailed functional changes (Fig. 4D). Cellular senescence reduced the basal respiration which is required to satisfy the ATP demand from mitochondrial proton leak (Fig. 4E). ATP production and spare respiratory capacity were also decreased (Fig. 4E, 4F). The reduced ATP levels enhanced the oxidative damage, increased the ROS generation, or increased the mtDNA mutation, in which all could induce mitochondrial damage (Srivastava, 2017). Mitochondrial dysfunction in astrocytes could lead to abnormality in the extracellular environment maintenance, which is expected to directly or indirectly affect neurons. MAO-B is located in the outer mitochondrial membrane and plays an important role in the catabolism of neuroactive and vasoactive amines in the central nervous system (CNS) and peripheral tissues. MAO-B expression is specifically found in astrocytes during adulthood CNS (Saura *et al*., 1992) and increases with age (Kumar and Andersen, 2004). MAO-B creates ROS, which known to affect cell damage directly (Nagatsu and Sawada, 2006) and MAO-B is highly implicated in the pathogenesis of Alzheimer's disease and Parkinson's disease (Saura *et al*., 1994; Mallajosyula *et al*., 2009). For example, in the astrocytes of an AD mouse model, the synthesis of GABA via activation of MAO-B affected neuronal activity and memory ability (Jo *et al*., 2014).

Moving forward from this study, it is necessary to confirm the mechanisms of mitochondrial dysregulation and MAO-B related signals and factors. Moreover, drug screening of antioxidants which could reverse aging will be of great interest. Our data suggest that etoposide can induce mitochondrial dysfunction and cellular senescence in astrocytes and could provide mechanistic insights in brain aging and neurodegenerative diseases. Aging astrocytes are known to represent mainly reactive or activated astrocytes, especially A1 astrocytes, which are recently identified as additional molecular profiles of aged astrocytes (Liddelow *et al*., 2017; Boisvert *et al*., 2018; Clarke *et al*., 2018). Changes in gene expression profile in aging astrocytes overlap with those in reactive astrocytes (Boisvert *et al*., 2018). Thus, further studies of aged astrocytes in the context of the relationship between etoposide-treated astrocytes and reactive astrocytes are an important subject to delve.

ACKNOWLEDGMENTS

This work was supported by Basic Science Research Program through the National Research Foundation of Korea (NRF) funded by the Ministry of Science, ICT & Future Planning (NRF-2016R1A2B4014707) and the Korea government (NRF-2016R1A5A2012284).

REFERENCES

Abbott, N. J. (2002) Astrocyte-endothelial interactions and blood-brain barrier permeability. *J. Anat.* **200**, 629-638.

Amodeo, A. A. and Skotheim, J. M. (2016) Cell-size control. *Cold Spring Harb. Perspect. Biol.* **8**, a019083.

Bang, M., Ryu, O., Kim, D. G., Mabunga, D. F., Cho, K. S., Kim, Y., Han, S. H., Kwon, K. J. and Shin, C. Y. (2018) Tenovin-1 induces senescence and decreases wound-healing activity in cultured rat primary astrocytes. *Biomol. Ther. (Seoul)* **27**, 283-289.

Bhat, R., Crowe, E. P., Bitto, A., Moh, M., Katsetos, C. D., Garcia, F. U., Johnson, F. B., Trojanowski, J. Q., Sell, C. and Torres, C. (2012) Astrocyte senescence as a component of Alzheimer's disease. *PLoS ONE* **7**, e45069.

Bialas, A. R. and Stevens, B. (2013) TGF-beta signaling regulates neuronal C1q expression and developmental synaptic refinement. *Nat. Neurosci.* **16**, 1773-1782.

Boisvert, M. M., Erikson, G. A., Shokhirev, M. N. and Allen, N. J. (2018) The aging astrocyte transcriptome from multiple regions of the mouse brain. *Cell Rep.* **22**, 269-285.

Burda, J. E., Bernstein, A. M. and Sofroniew, M. V. (2016) Astrocyte roles in traumatic brain injury. *Exp. Neurol.* **275 Pt 3**, 305-315.

Campbell, I. L., Abraham, C. R., Masliah, E., Kemper, P., Inglis, J. D., Oldstone, M. B. and Mucke, L. (1993) Neurologic disease induced in transgenic mice by cerebral overexpression of interleukin 6. *Proc. Natl. Acad. Sci. U.S.A.* **90**, 10061-10065.

Campisi, J., Andersen, J. K., Kapahi, P. and Melov, S. (2011) Cellular senescence: a link between cancer and age-related degenerative disease? *Semin. Cancer Biol.* **21**, 354-359.

Campuzano, O., Castillo-Ruiz, M. M., Acarin, L., Castellano, B. and Gonzalez, B. (2009) Increased levels of proinflammatory cytokines in the aged rat brain attenuate injury-induced cytokine response after excitotoxic damage. *J. Neurosci. Res.* **87**, 2484-2497.

Capell, B. C., Drake, A. M., Zhu, J., Shah, P. P., Dou, Z., Dorsey, J., Simola, D. F., Donahue, G., Sammons, M., Rai, T. S., Natale, C., Ridky, T. W., Adams, P. D. and Berger, S. L. (2016) MLL1 is essential for the senescence-associated secretory phenotype. *Genes Dev.* **30**, 321-336.

Chang, H. N., Pang, J. H., Chen, C. P., Ko, P. C., Lin, M. S., Tsai, W. C. and Yang, Y. M. (2012) The effect of aging on migration, proliferation, and collagen expression of tenocytes in response to ciprofloxacin. *J. Orthop. Res.* **30**, 764-768.

Chung, W. S., Clarke, L. E., Wang, G. X., Stafford, B. K., Sher, A., Chakraborty, C., Joung, J., Foo, L. C., Thompson, A., Chen, C., Smith, S. J. and Barres, B. A. (2013) Astrocytes mediate synapse elimination through MEGF10 and MERTK pathways. *Nature* **504**, 394-400.

Chung, W. S., Welsh, C. A., Barres, B. A. and Stevens, B. (2015) Do glia drive synaptic and cognitive impairment in disease? *Nat. Neurosci.* **18**, 1539-1545.

Clarke, L. E., Liddelow, S. A., Chakraborty, C., Munch, A. E., Heiman, M. and Barres, B. A. (2018) Normal aging induces A1-like astrocyte reactivity. *Proc. Natl. Acad. Sci. U.S.A.* **115**, E1896-E1905.

Collins-Hooper, H., Woolley, T. E., Dyson, L., Patel, A., Potter, P., Baker, R. E., Gaffney, E. A., Maini, P. K., Dash, P. R. and Patel, K. (2012) Age-related changes in speed and mechanism of adult skeletal muscle stem cell migration. *Stem Cells* **30**, 1182-1195.

Dai, W., Zhou, J., Jin, B. and Pan, J. (2016) Class III-specific HDAC inhibitor Tenovin-6 induces apoptosis, suppresses migration and eliminates cancer stem cells in uveal melanoma. *Sci. Rep.* **6**, 22622.

De Cecco, M., Jeyapalan, J., Zhao, X., Tamamori-Adachi, M. and Sedivy, J. M. (2011) Nuclear protein accumulation in cellular senescence and organismal aging revealed with a novel single-cell resolution fluorescence microscopy assay. *Aging (Albany N.Y.)* **3**, 955-967.

Dimri, G. P., Lee, X., Basile, G., Acosta, M., Scott, G., Roskelley, C., Medrano, E. E., Linskens, M., Rubelj, I., Pereira-Smith, O., Peacocke, M. and Campisi, J. (1995) A biomarker that identifies senescent human cells in culture and in aging skin *in vivo*. *Proc. Natl. Acad. Sci. U.S.A.* **92**, 9363-9367.

Dossi, E., Vasile, F. and Rouach, N. (2018) Human astrocytes in the diseased brain. *Brain Res. Bull.* **136**, 139-156.

Enokido, Y., Yoshitake, A., Ito, H. and Okazawa, H. (2008) Age-dependent change of HMGB1 and DNA double-strand break accumulation in mouse brain. *Biochem. Biophys. Res. Commun.* **376**, 128-133.

Fiacco, T. A., Agulhon, C. and McCarthy, K. D. (2009) Sorting out astrocyte physiology from pharmacology. *Annu. Rev. Pharmacol. Toxicol.* **49**, 151-174.

Godbout, J. P. and Johnson, R. W. (2004) Interleukin-6 in the aging brain. *J. Neuroimmunol.* **147**, 141-144.

Grolleau-Julius, A., Harning, E. K., Abernathy, L. M. and Yung, R. L. (2008) Impaired dendritic cell function in aging leads to defective antitumor immunity. *Cancer Res.* **68**, 6341-6349.

Hayflick, L. and Moorhead, P. S. (1961) The serial cultivation of human diploid cell strains. *Exp. Cell Res.* **25**, 585-621.

Hou, J., Cui, C., Kim, S., Sung, C. and Choi, C. (2018) Ginsenoside F1 suppresses astrocytic senescence-associated secretory phenotype. *Chem. Biol. Interact.* **283**, 75-83.

Hu, W., Huang, X. S., Wu, J. F., Yang, L., Zheng, Y. T., Shen, Y. M., Li, Z. Y. and Li, X. (2018) Discovery of novel topoisomerase II inhibitors by medicinal chemistry approaches. *J. Med. Chem.* **61**, 8947-8980.

Hudgins, A. D., Tazearslan, C., Tare, A., Zhu, Y., Huffman, D. and Suh, Y. (2018) Age- and tissue-specific expression of senescence biomarkers in mice. *Front. Genet.* **9**, 59.

Jo, S., Yarishkin, O., Hwang, Y. J., Chun, Y. E., Park, M., Woo, D. H., Bae, J. Y., Kim, T., Lee, J., Chun, H., Park, H. J., Lee, D. Y., Hong, J., Kim, H. Y., Oh, S. J., Park, S. J., Lee, H., Yoon, B. E., Kim, Y., Jeong, Y., Shim, I., Bae, Y. C., Cho, J., Kowall, N. W., Ryu, H., Hwang, E., Kim, D. and Lee, C. J. (2014) GABA from reactive astrocytes impairs memory in mouse models of Alzheimer's disease. *Nat. Med.* **20**, 886-896.

Kalman, J., Juhasz, A., Laird, G., Dickens, P., Jardanhazy, T., Rimanoczy, A., Boncz, I., Parry-Jones, W. L. and Janka, Z. (1997) Serum interleukin-6 levels correlate with the severity of dementia in Down syndrome and in Alzheimer's disease. *Acta Neurol. Scand.* **96**, 236-240.

Kim, J. N., Kim, M. K., Cho, K. S., Choi, C. S., Park, S. H., Yang, S. I., Joo, S. H., Park, J. H., Bahn, G., Shin, C. Y., Lee, H. J., Han, S. H. and Kwon, K. J. (2013) Valproic acid regulates alpha-synuclein expression through JNK pathway in rat primary astrocytes. *Biomol. Ther. (Seoul)* **21**, 222-228.

Kumar, M. J. and Andersen, J. K. (2004) Perspectives on MAO-B in aging and neurological disease: where do we go from here? *Mol. Neurobiol.* **30**, 77-89.

Liddelow, S. A., Guttenplan, K. A., Clarke, L. E., Bennett, F. C., Bohlen, C. J., Schirmer, L., Bennett, M. L., Munch, A. E., Chung, W. S., Peterson, T. C., Wilton, D. K., Frouin, A., Napier, B. A., Panicker, N., Kumar, M., Buckwalter, M. S., Rowitch, D. H., Dawson, V. L., Dawson, T. M., Stevens, B. and Barres, B. A. (2017) Neurotoxic reactive astrocytes are induced by activated microglia. *Nature* **541**, 481-487.

Mallajosyula, J. K., Chinta, S. J., Rajagopalan, S., Nicholls, D. G. and Andersen, J. K. (2009) Metabolic control analysis in a cellular model of elevated MAO-B: relevance to Parkinson's disease. *Neurotox. Res.* **16**, 186-193.

McHugh, D. and Gil, J. (2018) Senescence and aging: Causes, consequences, and therapeutic avenues. *J. Cell Biol.* **217**, 65-77.

Meyer, P., Maity, P., Burkovski, A., Schwab, J., Mussel, C., Singh, K., Ferreira, F. F., Krug, L., Maier, H. J., Wlaschek, M., Wirth, T., Kestler, H. A. and Scharffetter-Kochanek, K. (2017) A model of the onset of the senescence associated secretory phenotype after DNA

damage induced senescence. *PLoS Comput. Biol.* **13**, e1005741.
Nagatsu, T. and Sawada, M. (2006) Molecular mechanism of the relation of monoamine oxidase B and its inhibitors to Parkinson's disease: possible implications of glial cells. *J. Neural Transm. Suppl.* **(71)**, 53-65.
Nasrin Ghassemi, B. and Shokrzadeh, M. D. (2018) Protective effect of amifostine against etoposide-induced genotoxicity evaluated by the comet assays. *SOJ Pharm. Pharm. Sci.* **5**, 1-5.
Ortiz-Montero, P., Londono-Vallejo, A. and Vernot, J. P. (2017) Senescence-associated IL-6 and IL-8 cytokines induce a self- and cross-reinforced senescence/inflammatory milieu strengthening tumorigenic capabilities in the MCF-7 breast cancer cell line. *Cell Commun. Signal.* **15**, 17.
Pommier, Y., Leo, E., Zhang, H. and Marchand, C. (2010) DNA topoisomerases and their poisoning by anticancer and antibacterial drugs. *Chem. Biol.* **17**, 421-433.
Qiu, Z., Sweeney, D. D., Netzeband, J. G. and Gruol, D. L. (1998) Chronic interleukin-6 alters NMDA receptor-mediated membrane responses and enhances neurotoxicity in developing CNS neurons. *J. Neurosci.* **18**, 10445-10456.
Salminen, A., Ojala, J., Kaarniranta, K., Haapasalo, A., Hiltunen, M. and Soininen, H. (2011) Astrocytes in the aging brain express characteristics of senescence-associated secretory phenotype. *Eur. J. Neurosci.* **34**, 3-11.
Saura, J., Kettler, R., Da Prada, M. and Richards, J. G. (1992) Quantitative enzyme radioautography with 3H-Ro 41-1049 and 3H-Ro 19-6327 *in vitro*: localization and abundance of MAO-A and MAO-B in rat CNS, peripheral organs, and human brain. *J. Neurosci.* **12**, 1977-1999.
Saura, J., Luque, J. M., Cesura, A. M., Da Prada, M., Chan-Palay, V., Huber, G., Loffler, J. and Richards, J. G. (1994) Increased monoamine oxidase B activity in plaque-associated astrocytes of Alzheimer brains revealed by quantitative enzyme radioautography. *Neuroscience* **62**, 15-30.
Srivastava, S. (2017) The mitochondrial basis of aging and age-related disorders. *Genes (Basel)* **8**, E398.
te Poele, R. H., Okorokov, A. L., Jardine, L., Cummings, J. and Joel, S. P. (2002) DNA damage is able to induce senescence in tumor cells *in vitro* and *in vivo*. *Cancer Res.* **62**, 1876-1883.
Vallieres, L., Campbell, I. L., Gage, F. H. and Sawchenko, P. E. (2002) Reduced hippocampal neurogenesis in adult transgenic mice with chronic astrocytic production of interleukin-6. *J. Neurosci.* **22**, 486-492.
Voloboueva, L. A., Suh, S. W., Swanson, R. A. and Giffard, R. G. (2007) Inhibition of mitochondrial function in astrocytes: implications for neuroprotection. *J. Neurochem.* **102**, 1383-1394.
Woodroofe, M. N., Sarna, G. S., Wadhwa, M., Hayes, G. M., Loughlin, A. J., Tinker, A. and Cuzner, M. L. (1991) Detection of interleukin-1 and interleukin-6 in adult rat brain, following mechanical injury, by *in vivo* microdialysis: evidence of a role for microglia in cytokine production. *J. Neuroimmunol.* **33**, 227-236.
Yoon, K. B., Park, K. R., Kim, S. Y. and Han, S. Y. (2016) Induction of nuclear enlargement and senescence by sirtuin inhibitors in glioblastoma cells. *Immune Netw.* **16**, 183-188.